

## RESEARCH ARTICLE

# OpenDSS-Based Harmonic Power Flow Analysis for Distribution Systems With Passive Power Filters

NIEN-CHE YANG<sup>ID</sup>, (Member, IEEE), AND YU-WEI HSU<sup>ID</sup>

Department of Electrical Engineering, National Taiwan University of Science and Technology, Taipei 10607, Taiwan

Corresponding author: Nien-Che Yang (ncyang@mail.ntust.edu.tw)

This work was supported in part by the National Science and Technology Council (NSTC) of Taiwan, in part by NSTC under Grant NSTC 111-2622-8-011-014-SB, in part by Delta Electronics (DELTA), and in part by the National Taiwan University of Science of Technology (NTUST) Joint Research Center.

**ABSTRACT** The open distribution system simulator (OpenDSS) is open-source software developed by the Electric Power Research Institute (EPRI) in the United States for analyzing distribution systems. OpenDSS is primarily used in distribution systems for fundamental power flow (FPF) and harmonic power flow (HPF). Single-tune and high-order filters are generally combined to achieve a better harmonic filtering performance in practical harmonic analysis applications. However, OpenDSS requires high-order filter models. This hinders the simulation of comprehensive and reliable filtering results. Moreover, HPF calculation errors occur when shunt components and power systems exhibit harmonic resonance. This paper proposes passive power filter models based on the injected current technique to compensate for the deficiency of high-order filters in OpenDSS. Furthermore, the proposed method can effectively prevent parallel harmonic resonance errors. This results in higher accuracy and practicability of the HPF and passive power filters (PPFs) models in distribution systems.

**INDEX TERMS** Admittance matrix, fundamental power flow, harmonic power flow, harmonic resonance, passive filter, nonlinear loads.

## I. INTRODUCTION

The increasing use of nonlinear loads in power systems has resulted in harmonic currents that contribute to system power losses and cause problems such as overheating, waveform distortion, and communication interference [1]. To address these power quality issues, power system simulation software is required to analyze the fundamental power flow (FPF) and harmonic power flow (HPF). An accurate analysis requires an effective design of the component models. However, in current research and power system simulation software, the component models are generally assumed to be linear, and the nonlinearity is omitted almost completely. This may result in significant errors in the HPF analysis [2]. Nonlinear loads may inject harmonic currents into the distribution system,

and inaccurate component modeling can result in impedance calculation errors. This causes harmonic voltage calculation errors. Thus, an effective modeling of the components and consideration of their nonlinearities is essential [3].

To address power quality problems, shunt capacitors (SCs) or harmonic filters are typically installed in distribution systems for power factor correction and reactive power compensation [4]. Harmonic filters can be categorized into passive filters (PPFs) and active filters (APFs). PPFs have a simple structure, primarily consisting of resistors (R), capacitors (C), and inductors (L). They are inexpensive and suitable for fixed loads. APFs generate corresponding reverse harmonic signals by detecting harmonic components in power systems to cancel or suppress harmonic currents [5]. APFs have a complex structure, difficult design process, and the risk of internal electronic component failure. Currently, PPFs are commonly used in the industry instead of

The associate editor coordinating the review of this manuscript and approving it for publication was Dinesh Kumar.

APFs. However, the installation of SCs or PPFs can result in harmonic resonances in distribution systems. When harmonic resonance occurs in distribution systems, the accuracy and convergence of the HPF are affected by the component models [6]. The HPF can be analyzed using single-phase, multiphase, alternate iteration, and decoupling methods. Conventional HPF methods such as Newton–Raphson [7] and Y-bus Gaussian [8] have been widely used in power system analyses for many decades. However, these are slow for larger power systems because these require a lower and upper (LU) decomposition of the system bus admittance matrix and the solving of the inverse matrix to obtain the system bus impedance matrix. If the power system experiences harmonic resonance, the system bus admittance matrix becomes singular. This results in errors in the inverse matrix solution. In addition to these conventional methods, the backward/forward sweep-based (BFSB) method [9] is effective for power system analysis. By computing and iteratively solving the responses of the linear and nonlinear components in two stages, the time-consuming LU decomposition required to solve the inverse matrix can be circumvented. However, when harmonic resonance occurs in a power system, the iterative process of the BFSB becomes slow (particularly when higher-order harmonics occur), and the system impedance near the resonance frequency becomes small. This necessitates thousands of iterations to converge and thereby, long computation times. A three-phase power-flow method for unbalanced distribution systems was proposed [10] to construct a system bus impedance matrix directly using the graph theory. This eliminated the need for matrix inversion. Moreover, divergence problems under harmonic resonance conditions can be prevented using the injected current for the shunt components. Therefore, a comprehensive HPF analysis of power systems should consider the nonlinear components and HPF methods.

The open distribution system simulator (OpenDSS) has been incorporated with FPF and HPF algorithms. However, similar to the conventional HPF algorithms, errors may occur if harmonic resonances exist in power systems. Furthermore, OpenDSS does not have high-order filter models. This limits its practicality in the HPF analysis of distribution systems. This study proposed a modification program that integrates PPF models into OpenDSS to address these issues. The modification programs improved the FPF and HPF algorithms. Thereby, these prevented errors in the HPF calculations caused by harmonic resonances.

The remainder of this paper is organized as follows. Section II presents the problems caused by harmonic resonance and defines the harmonic indicators used in this study. Section III describes the network components and PPFs models used in the test systems. Section IV presents the FPF and HPF algorithms in OpenDSS in conjunction with the proposed methods. Section V reports the test results for the two test systems and analyzes the practicality of the proposed method. Finally, Section VI provides the conclusions.

## II. BASIC CONCEPTS

Conventional HPF methods rely on solving the inverse matrix of the system bus admittance matrix to obtain the bus impedance matrix. However, the harmonic resonance in a power system can cause errors in inverse matrix calculations. This section briefly overviews the issues caused by harmonic resonance and the harmonic indices used in this study.

### A. EIGENVALUE DECOMPOSITION

To solve the inverse of the bus admittance matrix using eigenvalue decomposition, the system bus admittance matrix  $\mathbf{Y}_{\text{bus}}$  when the power system has  $i$  buses is represented as (1):

$$\mathbf{Y}_{\text{bus}} = \begin{bmatrix} y_{11} & \cdots & y_{1i} \\ \vdots & \ddots & \vdots \\ y_{i1} & \cdots & y_{ii} \end{bmatrix}_{i \times i} \quad (1)$$

If the effect of the phase shift on the transformers is omitted,  $\mathbf{Y}_{\text{bus}}$  becomes a symmetric matrix. Therefore, the eigenvalues and eigenvectors can decompose  $\mathbf{Y}_{\text{bus}}$  as shown in (2):

$$\mathbf{Y}_{\text{bus}} = \mathbf{L} \mathbf{\Lambda} \mathbf{T} \quad (2)$$

The left and right eigenvector matrices of  $\mathbf{Y}_{\text{bus}}$  are denoted as  $\mathbf{L}$  and  $\mathbf{T}$ , respectively, as shown in (3):

$$\mathbf{L} = \mathbf{T}^t = \begin{bmatrix} \vdots & \cdots & \vdots \\ l_1 & \cdots & l_i \\ \vdots & \cdots & \vdots \end{bmatrix}_{i \times i} \quad (3)$$

$\mathbf{\Lambda}$  is a diagonal matrix representing the eigenvalue matrix of  $\mathbf{Y}_{\text{bus}}$ , as shown in (4):

$$\mathbf{\Lambda} = \begin{bmatrix} \lambda_1 & \cdots & 0 \\ \vdots & \ddots & \vdots \\ 0 & \cdots & \lambda_i \end{bmatrix}_{i \times i} \quad (4)$$

If all the eigenvalues of  $\mathbf{Y}_{\text{bus}}$  are nonzero,  $\mathbf{Y}_{\text{bus}}$  is a nonsingular matrix that can be decomposed into eigenvalue and eigenvector matrices. This enables the calculation of its inverse. Applying eigenvalue decomposition to power systems can aid in understanding the harmonic behavior and oscillation problems of power systems. The eigenvalues and eigenvectors provide information regarding the amplitude and phase characteristics of each node in the power system. According to [11], certain eigenvalues tend toward zero during harmonic resonance in power systems. In such cases,  $\mathbf{Y}_{\text{bus}}$  becomes singular or nearly singular and cannot be diagonalized. This renders an inverse calculation infeasible. Furthermore, if the power system oscillates, the eigenvalues may become multiple roots, and the inverse matrix cannot be computed. Therefore, the conventional HPF results in significant errors when the system experiences a harmonic resonance.

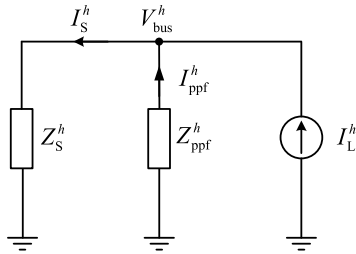


FIGURE 1. Single phase diagram of a system with a PPF and nonlinear load.

**B. HARMONIC INDICES**

Harmonic indices are crucial parameters for assessing the power quality of power systems. The harmonic indices used in this study consist of the total voltage harmonic distortion (TVHD), individual voltage harmonic distortion (IVHD), and harmonic current gain ( $G_I$ ).

Assuming the  $H^{th}$  harmonic order in the harmonic source,  $TVHD_i$  is defined as the ratio of the root mean square (RMS) value of the harmonic voltage components on the  $i$ th bus to that of the fundamental voltage component (see (5)):

$$TVHD_i = \frac{\sqrt{\sum_{h=2}^H (V_i^h)^2}}{V_i^{h=1}} \tag{5}$$

The individual voltage harmonic distortion (IVHD) is defined as the ratio of the RMS value of the  $h^{th}$ -order harmonic voltage component on the  $i$ th bus to that of the fundamental voltage component, as shown in (6):

$$IVHD_i^h = \frac{V_i^h}{V_i^{h=1}} \tag{6}$$

The harmonic current gain ( $G_I$ ) is defined as the ratio of the injected current  $I_S^h$  to the harmonic current  $I_L^h$  in the power system, as expressed in (7):

$$G_I^h = \frac{|I_S^h|}{|I_L^h|} = \frac{|Z_{ppf}^h|}{|Z_S^h + Z_{ppf}^h|} \tag{7}$$

A typical system with PPF impedance  $Z_{ppf}^h$  and equivalent driving-point impedance  $Z_S^h$  is shown in Figure 1. When a harmonic current  $I_L^h$  flows through a shunt component containing an SC, the branch-sharing effect may result in a harmonic current  $I_S^h$  higher than  $I_L^h$ . This generates a harmonic current gain  $G_I^h$  higher than one. When harmonic resonance occurs between the power system and SC,  $|Z_S^h + Z_{ppf}^h|$  approaches zero, and  $G_I^h$  becomes significantly large. The harmonic current gain  $G_I^h$  clearly indicates whether the harmonic resonance at a particular bus causes the amplification of harmonic currents.

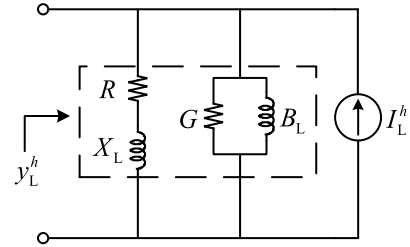


FIGURE 2. Single phase harmonic load model.

**III. COMPONENTS MODELS**

This section describes the component models used in this study. The transmission line and load demand models used for the PPF and HPF are based on the OpenDSS default models [12]. However, we propose an equivalent-injected current-based model for PPFs.

**A. TRANSMISSION LINE MODEL**

In OpenDSS, the transmission line is represented by an equivalent  $\pi$  model. The inductance and mutual inductance of each phase can be calculated using Carson’s equations [13]. Subsequently, the equivalent series impedance matrix  $Z_{line}^{abc}$  can be calculated using Kron reduction, as shown in (8):

$$Z_{line}^{abc} = \begin{bmatrix} Z^{aa-g} & Z^{ab-g} & Z^{ac-g} \\ Z^{ba-g} & Z^{bb-g} & Z^{bc-g} \\ Z^{ca-g} & Z^{cb-g} & Z^{cc-g} \end{bmatrix} \tag{8}$$

The series impedance  $Z_{line}^{abc}$  consists of the resistance  $R_{line}$  and inductive reactance  $X_{line}$  in series, as shown in (9):

$$Z_{line} = R_{line} + j \cdot X_{line} \tag{9}$$

In the HPF, the transmission line model is a linear impedance that varies with the frequency. Thus, the series impedance elements of the transmission line can be expressed for the  $h^{th}$  harmonic order, as shown in (10):

$$Z_{line}^h = R_{line} + jh \cdot X_{line} \tag{10}$$

**B. LOAD MODEL**

The load model in the OpenDSS is an aggregated load model. Based on the load phase, the loads can be categorized into single- and three-phase loads. The load connection can be divided into Y-type and  $\Delta$ -type. The load type can be divided into constant power, current, and impedance loads. The load model used in this study is a three-phase Y-type constant-power load. In the PPF, the rated load impedance  $Z_{rated}^\varphi$  was determined using the rated voltage  $V_{rated}^\varphi$  and rated power  $S_{rated}^\varphi$ , as shown in (11):

$$Z_{rated}^\varphi = \frac{|V_{rated}^\varphi|^2}{S_{rated}^\varphi}, \quad \varphi \in \{a, b, c\} \tag{11}$$

In the PPF, the load current  $I^\varphi$  for a constant load is

$$I^\varphi = \left( \frac{S_{rated}^\varphi}{V^\varphi} \right)^* \tag{12}$$

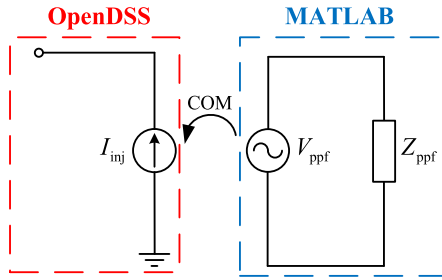


FIGURE 3. Injected current-based model.

During the iteration process,  $S_{\text{rated}}^{\varphi}$  remains constant, and the phase voltage  $V^{\varphi}$  is updated continuously until convergence.

In the HPF, the load model in OpenDSS is considered a Norton equivalent circuit, as shown in Figure 2.

The linear part of the load demand is equivalent to a linear admittance  $y_L^h$  consisting of shunt and series admittances, as shown in (13):

$$y_L^h = \rho \cdot \left( G + \frac{j \cdot B_L}{h} \right) + (1 - \rho) \cdot \left( \frac{1}{R + j \cdot h \cdot X_L} \right) \quad (13)$$

where  $\rho$  is the shunt-series admittance proportion (50% in this study).

The nonlinear part was modeled using an injected current source. According to the harmonic properties, the  $h^{\text{th}}$ -order harmonic current  $I_L^h$  is a fraction of the fundamental current  $I_L^{h=1}$ . The magnitude of  $I_L^h$  is calculated based on the specified harmonic spectrum  $I_{\text{spectrum}}^h$ , as shown in (14):

$$I_L^h = I_L^{h=1} \cdot I_{\text{spectrum}}^h \quad (14)$$

The angle of the harmonic current  $\theta_L^h$  can be calculated using (15):

$$\theta_L^h = h \cdot \theta_L^{h=1} + \theta_{\text{spectrum}}^h \quad (15)$$

### C. PASSIVE POWER FILTER MODEL

Most studies of PPFs have considered these as linear elements. The equivalent impedance is integrated into the system bus admittance matrix,  $\mathbf{Y}_{\text{bus}}$ . However, as demonstrated in Section II, when the PPFs are in harmonic resonance with the power system,  $\mathbf{Y}_{\text{bus}}$  becomes a singular matrix. This enables solving of the harmonic voltages using inverse matrix computation. Significant errors may occur while performing PPF and HPF. Therefore, an injected-current source-based model was proposed for the PPFs. The current source model does not affect the singularity of  $\mathbf{Y}_{\text{bus}}$ , thereby preventing the aforementioned problems.

OpenDSS supports several third-party software applications such as MATLAB and Python via the component object model (COM) interface [14]. This enables the transfer and modification of parameters in OpenDSS component models. The PPF model was set in MATLAB to evaluate the equivalent injected currents. Using the COM interface, the

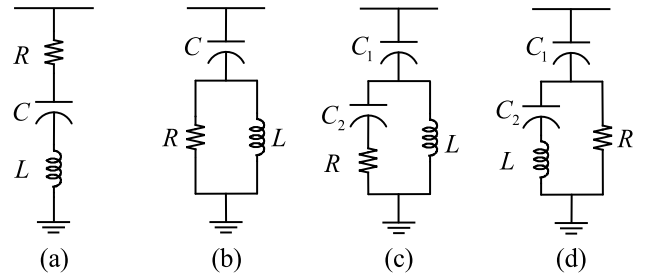


FIGURE 4. Typical PPFs: (a) single-tuned PPF (b) second-order damped PPF (c) third-order damped PPF and (d) C-type damped PPF.

PPFs model in OpenDSS was represented as a current-source-based model (see Figure 3).

PPFs can be classified into two categories: single- and higher-order filters. High-order damped filters can be classified further into second-, third-, and C-type filters, as shown in Figure 4.

The inductive reactance of PPFs at the fundamental frequency  $f$  is

$$X_L = 2\pi fL \quad (16)$$

The capacitive reactance of PPFs at the fundamental frequency  $f$  is

$$X_C = \frac{1}{2\pi fC} \quad (17)$$

The PPF impedance  $Z_{\text{ppf}}^h$  at the  $h^{\text{th}}$ -order harmonic frequency can be determined from the resistance  $R$ , inductive reactance  $X_L$ , and capacitive reactance  $X_C$ .

#### (a) Single-tuned PPF

In Figure 4(a), the single-tuned PPF consists of  $R$ ,  $L$ , and  $C$  connected in series. The single-tuned PPF offers the best filtering efficiency, capable of directly eliminating specific harmonics. It has a simple structure and low cost. However, component designing should be done cautiously to avoid component overload and harmonic resonance problems. The impedance can be calculated using (18):

$$Z_{\text{ppf}}^h = R + j(hX_L - \frac{X_C}{h}) \quad (18)$$

#### (b) Second-order damped PPF

In Figure 4(b), the second-order PPF connects  $R$  and  $L$  in parallel and then, in series with  $C$ . The second-order PPF is widely used in the industry as a high-pass filter owing to its wide and low-impedance bandwidth characteristics. It has a wide range of harmonic current absorption and a low probability of harmonic resonance with a power system. The impedance can be calculated using (19):

$$Z_{\text{ppf}}^h = \frac{R(hX_L)^2}{R^2 + (hX_L)^2} + j\left[ \frac{R^2 hX_L}{R^2 + (hX_L)^2} - \frac{X_C}{h} \right] \quad (19)$$

#### (c) Third-order damped PPF

Figure 4 (c) shows that the third-order PPF differs from the second-order PPF in that  $C_2$  is connected in series with  $R$  and then, in parallel with  $L$ . When  $X_C = \frac{1}{2\pi fC_2}$  and

$C_1 = C_2$ . A third-order PPF is used to mitigate the significant power loss at the fundamental frequency in a second-order PPF. The higher overall impedance of the third-order PPF reduces the fundamental frequency current flowing through the resistor, thereby ameliorating the problem encountered with the second-order PPF. The impedance can be calculated using (20):

$$Z_{ppf}^h = \frac{R(hX_L)^2}{R^2 + \left(hX_L - \frac{X_C}{h}\right)^2} + j\left[\frac{R^2 hX_L - hX_L^2 X_C + \frac{X_L X_C^2}{h}}{R^2 + \left(hX_L - \frac{X_C}{h}\right)^2} - \frac{X_C}{h}\right] \quad (20)$$

(d) C-type PPF

Figure 4(d) shows that the C-type PPF differs from the third-order PPF in that  $C_2$  is connected in series with  $L$  and then, in parallel with  $R$ . When  $X_C = \frac{1}{2\pi f C_2}$  and  $C_1 = \frac{1}{(2\pi f)^2 L}$ . Another way to mitigate power losses in a second-order PPF is to design a C-type PPF with zero branch impedance at the fundamental frequency; thus avoiding power losses caused by the fundamental frequency current flowing through the resistor. The impedance can be calculated using (21):

$$Z_{ppf}^h = \frac{R\left(hX_L - \frac{X_L}{h}\right)^2}{R^2 + \left(hX_L - \frac{X_L}{h}\right)^2} + j\left[\frac{R^2\left(hX_L - \frac{X_L}{h}\right)}{R^2 + \left(hX_L - \frac{X_L}{h}\right)^2} - \frac{X_C}{h}\right] \quad (21)$$

Using (22), the equivalent injected current of the PPFs, denoted by  $I_{ppf}^h$ , can be calculated based on the voltage  $V_{ppf}^h$  at the bus where  $Z_{ppf}^h$  is installed. Here,  $Z_{ppf}^h$  is the impedance of the PPFs at the harmonic frequency  $h$ .

$$I_{ppf}^h = (Z_{ppf}^h)^{-1} \cdot V_{ppf}^h \quad (22)$$

After obtaining  $I_{ppf}^h$  in MATLAB, it was converted into an equivalent injected current  $I_{inj}^h$  in OpenDSS for the FPF and HPF studies. In this study, the proposed models were based on a COM interface for communication in OpenDSS and MATLAB. The impedances and equivalent injected currents for the PPFs were calculated in MATLAB. Then, the PPFs were considered as the current source-based model in OpenDSS for the FPF and HPF studies. Figure 5 shows the communication between OpenDSS and MATLAB.

IV. PROPOSED ALGORITHM

In this section, the proposed PPFs model is integrated into the FPF and HPF in OpenDSS to overcome the deficiency of high-order filter models and reduce the calculation errors caused by harmonic resonance in the HPF. First, the FPF and HPF in OpenDSS are introduced, and the improved processes proposed in this study are explained.

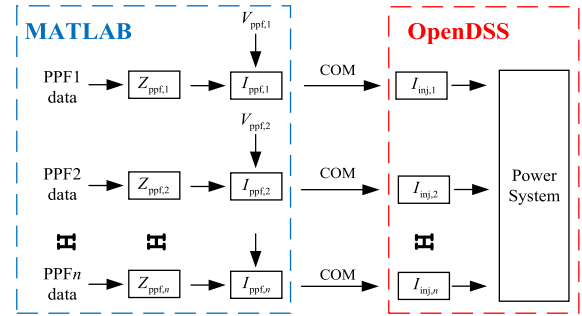


FIGURE 5. Communication between OpenDSS and MATLAB.

A. EXISTING ALGORITHM

The following is an introduction to the FPF and the HPF in OpenDSS.

1) OPENDSS FUNDAMENTAL POWER FLOW

The FPF in OpenDSS is similar to the conventional FPF method (i.e., the implicit Gauss method [15]) in that both begin with the primitive admittance matrix  $Y_{prim}$  for the component models and then, form the system bus admittance matrix  $Y_{bus}$ . Therefore, assuming a power system with  $i$  buses,  $Y_{bus}$  can be represented as (1).

In the OpenDSS, the injected current  $I_i$  is calculated based on the load demand, connected to the bus. Therefore, at the  $m$ -th iteration, the injected current vector  $I_{bus}^{(m)}$  is expressed as shown in (23):

$$I_{bus}^{(m)} = \begin{bmatrix} I_1^{(m)} \\ \vdots \\ I_i^{(m)} \end{bmatrix}_{i \times 1} \quad (23)$$

At the  $m$ -th iteration, the bus voltage vector matrix  $V_{bus}^{(m)}$  can be determined as

$$V_{bus}^{(m)} = (Y_{bus})^{-1} \cdot I_{bus}^{(m)} \quad (24)$$

where

$$V_{bus}^{(m)} = \begin{bmatrix} V_1^{(m)} \\ \vdots \\ V_i^{(m)} \end{bmatrix}_{i \times 1} \quad (25)$$

After solving for  $V_{bus}^{(m)}$ , the voltage mismatch  $\Delta V_{bus}^{(m)}$  at the  $m$ -th iteration can be calculated using (26):

$$\Delta V_{bus}^{(m)} = V_{bus}^{(m)} - V_{bus}^{(m-1)} \quad (26)$$

If  $\Delta V_{bus}^{(m)}$  is less than the iteration tolerance  $\epsilon$ ,  $V_{bus}^{(m)}$  is the converged solution. Otherwise, the iterative process continues. The bus-injected current vector  $I_{bus}^{(m+1)}$  is updated using  $V_{bus}^{(m)}$ . Then,  $V_{bus}^{(m+1)}$  can be calculated by repeating (24). This iterative process is repeated until convergence is achieved.



## 2) OPENDSS HARMONIC POWER FLOW

The HPF in OpenDSS is similar to the FPF in that it uses a decoupling method to compute the HPF solutions for each harmonic order independently. The harmonic-injected current vector  $\mathbf{I}_{\text{bus}}^h$  is formed by integrating  $I_{L,i}^h$  as shown in (27):

$$\mathbf{I}_{\text{bus}}^h = \begin{bmatrix} I_{L,1}^h \\ \vdots \\ I_{L,i}^h \end{bmatrix}_{i \times 1} \quad (27)$$

The bus admittance matrix  $\mathbf{Y}_{\text{bus}}^h$  at the  $h^{\text{th}}$ -order harmonic frequency is constructed for the power system. The harmonic voltage vector  $\mathbf{V}_{\text{bus}}^h$  can be determined directly without an iterative process in the HPF, as expressed in (28):

$$\mathbf{V}_{\text{bus}}^h = (\mathbf{Y}_{\text{bus}}^h)^{-1} \cdot \mathbf{I}_{\text{bus}}^h \quad (28)$$

The HPF in OpenDSS is known for its high accuracy in the initial voltage estimation and remarkable convergence. However, similar to the conventional HPF method discussed in Section II, it requires the computation of the inverse matrix of  $\mathbf{Y}_{\text{bus}}^h$  [16]. If  $\mathbf{Y}_{\text{bus}}^h$  is a singular or quasisingular matrix, the inverse matrix cannot be calculated. This results in significant errors in the voltage solutions.

## B. PROPOSED PROCESS

In this study, the double-loop iterative power flow method and direct  $Z_{\text{BUS}}$  harmonic power flow method [10], [17] were used to integrate the proposed PPF models into the FPF and HPF in OpenDSS. In addition, the  $G_1^h$  scanning method in OpenDSS was proposed to replace the conventional frequency-scanning method for analyzing the harmonic resonance frequency in power systems.

### 1) DOUBLE-LOOP ITERATIVE POWER FLOW

First, the PPFs impedance matrix  $\mathbf{Z}_{\text{ppf}}^{h=1}$  at the fundamental frequency was evaluated using the MATLAB software.  $\mathbf{Z}_{\text{ppf}}^{h=1}$  corresponds to the diagonal matrix. If  $n$  PPFs exist in the power system,  $\mathbf{Z}_{\text{ppf}}^{h=1}$  can be expressed as

$$\mathbf{Z}_{\text{ppf}}^{h=1} = \begin{bmatrix} Z_{\text{ppf},1}^{h=1} & \cdots & 0 \\ \vdots & \ddots & \vdots \\ 0 & \cdots & Z_{\text{ppf},n}^{h=1} \end{bmatrix}_{n \times n} \quad (29)$$

In addition, the initial bus voltage vector  $\mathbf{V}_{\text{bus}}^{(0)}$  is formulated as

$$\mathbf{V}_{\text{bus}}^{(0)} = \begin{bmatrix} V_1^{(0)} \\ \vdots \\ V_i^{(0)} \end{bmatrix}_{i \times 1} \quad (30)$$

The initial voltage vector at the bus with PPFs can be expressed as

$$\mathbf{V}_{\text{ppf}}^{(0)} = \begin{bmatrix} V_{\text{ppf},1}^{(0)} \\ \vdots \\ V_{\text{ppf},n}^{(0)} \end{bmatrix}_{n \times 1} \quad (31)$$

Therefore, at the  $k^{\text{th}}$  external loop iteration, the injected current vector  $\mathbf{I}_{\text{ppf}}^{(k)}$  of the PPFs is calculated as

$$\mathbf{I}_{\text{ppf}}^{(k)} = (\mathbf{Z}_{\text{ppf}}^{h=1})^{-1} \cdot \mathbf{V}_{\text{ppf}}^{(k)} \quad (32)$$

where

$$\mathbf{I}_{\text{ppf}}^{(k)} = \begin{bmatrix} I_{\text{ppf},1}^{(k)} \\ \vdots \\ I_{\text{ppf},n}^{(k)} \end{bmatrix}_{n \times 1} \quad (33)$$

The injected current source vector  $\mathbf{I}_{\text{inj}}^{(k)}$  in OpenDSS was obtained by transferring the  $\mathbf{I}_{\text{ppf}}^{(k)}$  to MATLAB. If no PPF is installed on the  $i^{\text{th}}$  bus, the element  $I_{\text{inj},i}^{(k)}$  in  $\mathbf{I}_{\text{inj}}^{(k)}$  is zero.  $\mathbf{I}_{\text{inj}}^{(k)}$  can be expressed as illustrated in (34):

$$\mathbf{I}_{\text{inj}}^{(k)} = \begin{bmatrix} I_{\text{inj},1}^{(k)} \\ \vdots \\ I_{\text{inj},i}^{(k)} \end{bmatrix}_{i \times 1} \quad (34)$$

At the  $m^{\text{th}}$  internal loop iteration, the bus voltage vector at the  $k^{\text{th}}$  external loop iteration can be expressed as shown in (35). After combining the original  $\mathbf{I}_{\text{bus}}$  in OpenDSS and the calculated  $\mathbf{I}_{\text{inj}}$  in MATLAB, an FPF calculation was performed using OpenDSS.

$$\mathbf{V}_{\text{bus}}^{(m,k)} = (\mathbf{Y}_{\text{bus}}^{h=1})^{-1} \cdot [\mathbf{I}_{\text{bus}}^{(m,k)} + \mathbf{I}_{\text{inj}}^{(k)}] \quad (35)$$

The voltage mismatch  $\Delta \mathbf{V}_{\text{bus}}^{(m,k)}$  in the internal loop is

$$\Delta \mathbf{V}_{\text{bus}}^{(m,k)} = \mathbf{V}_{\text{bus}}^{(m,k)} - \mathbf{V}_{\text{bus}}^{(m-1,k)} \quad (36)$$

If  $\Delta \mathbf{V}_{\text{bus}}^{(m,k)}$  is less than the preset iteration tolerance  $\varepsilon$ , the internal loop iteration converges. Otherwise,  $\mathbf{I}_{\text{bus}}^{(m+1,k)}$  is updated, and the internal loop iteration is repeated according to (35) until convergence is achieved. If the internal loop iteration converges,  $\mathbf{V}_{\text{bus}}^{(m,k)}$  is transferred to MATLAB as  $\mathbf{V}_{\text{bus}}^{(k)}$ , and the voltage mismatch  $\Delta \mathbf{V}_{\text{bus}}^{(k)}$  in the external loop is calculated using (37):

$$\Delta \mathbf{V}_{\text{bus}}^{(k)} = \mathbf{V}_{\text{bus}}^{(k)} - \mathbf{V}_{\text{bus}}^{(k-1)} \quad (37)$$

The external loop iteration converges if  $\Delta \mathbf{V}_{\text{bus}}^{(k)}$  is less than the preset iteration tolerance  $\varepsilon$ .  $\mathbf{V}_{\text{bus}}^{(k)}$  is the final converged voltage. Otherwise,  $\mathbf{V}_{\text{bus}}^{(k+1)}$  is updated using (38):

$$\mathbf{V}_{\text{bus}}^{(k+1)} = \mathbf{V}_{\text{bus}}^{(k)} + \Delta \mathbf{V}_{\text{bus}}^{(k)} \quad (38)$$

After updating  $\mathbf{V}_{\text{ppf}}^{(k+1)}$  based on  $\mathbf{V}_{\text{bus}}^{(k+1)}$ ,  $\mathbf{I}_{\text{ppf}}^{(k+1)}$  was updated by (32). The  $\mathbf{I}_{\text{ppf}}^{(k+1)}$  value calculated using MATLAB was used to update the  $\mathbf{I}_{\text{inj}}^{(k+1)}$  in OpenDSS. Moreover, the internal loop iteration was restarted based on (35). Both the loops converged. A flowchart of the double-loop iterative power flow is shown in Figure 6. The pseudocodes for Algorithms 1 and 2 are shown in Figure 7 and Figure 8, respectively.

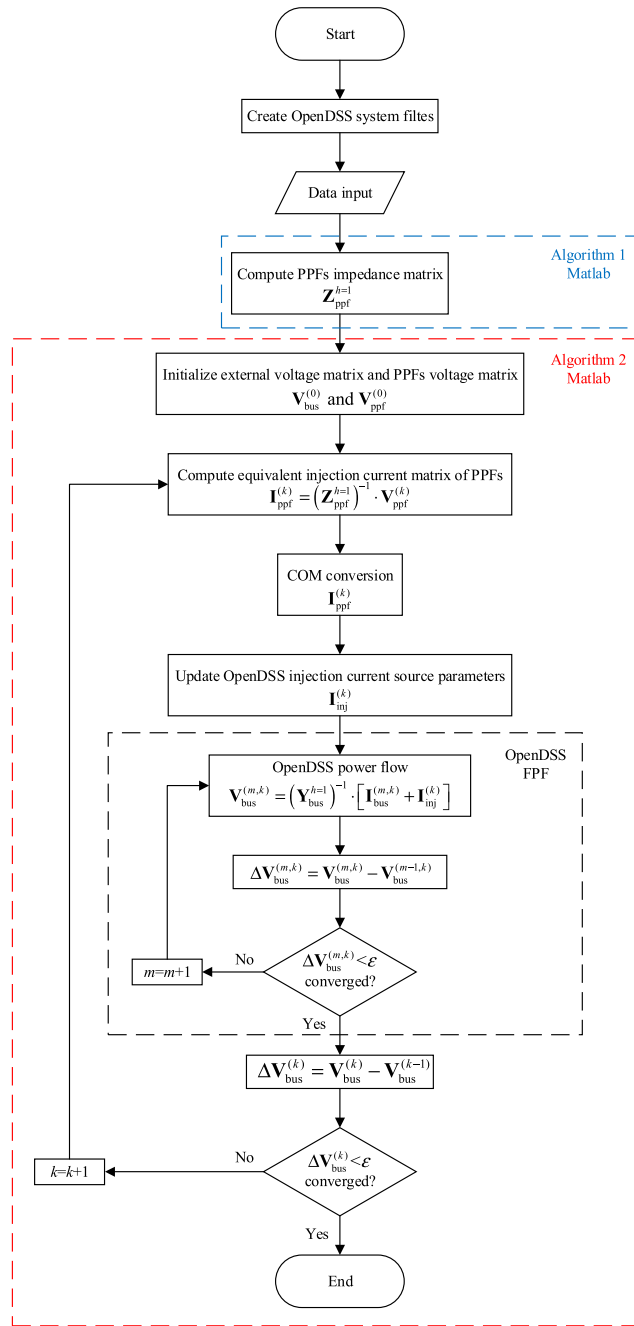


FIGURE 6. Flow chart of double-loop iterative power flow.

2) DIRECT Z<sub>BUS</sub> HARMONIC POWER FLOW

The direct Z<sub>BUS</sub> harmonic power flow method was developed based on the double-loop iterative power flow results. The load currents  $I_L^h$  and PPFs currents  $I_{ppf}^h$  can be integrated into the nonlinear load current vector  $I_L^h$  and PPFs model current vector  $I_{ppf}^h$ , respectively. Both the vectors can be integrated into the harmonic current injection vector  $I_S^h$ , as shown in (39). If the power system contains  $m$  harmonic loads and  $n$  PPFs, then  $I_L^h$  is an  $(m \times 1)$  vector,  $I_{ppf}^h$  is an  $(n \times 1)$  matrix, and  $I_S^h$  is an  $((m + n) \times 1)$  vector.  $I_L^h$  in OpenDSS can be

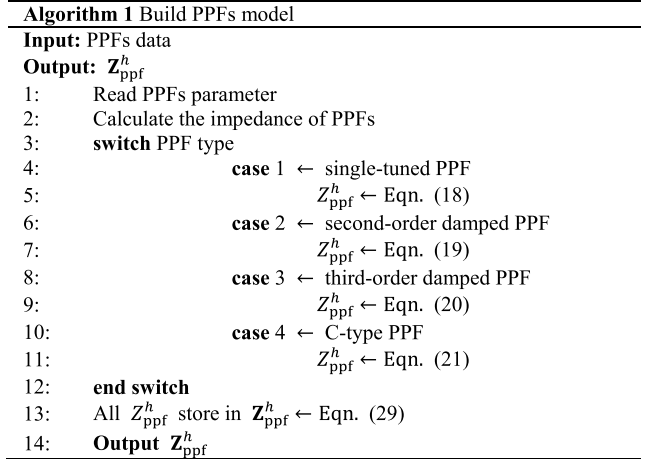


FIGURE 7. Pseudo-code-for algorithm 1.

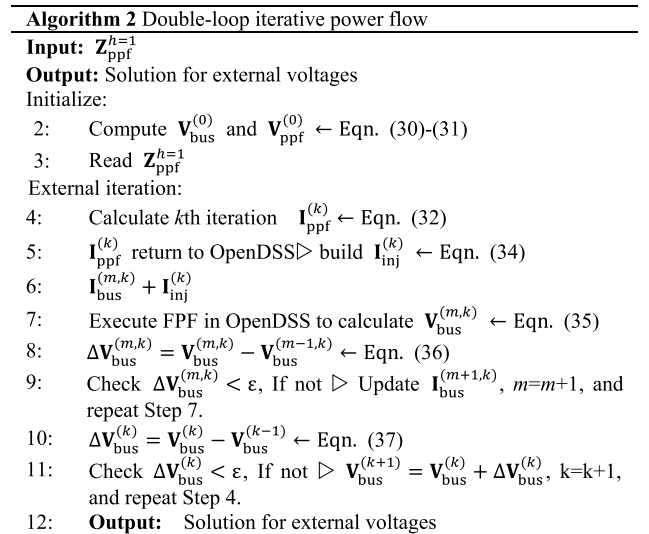


FIGURE 8. Pseudo-code-for Algorithm 2.

returned to MATLAB via the COM interface, whereas  $I_{ppf}^h$  can be calculated using MATLAB.

$$I_S^h = \begin{bmatrix} I_L^h \\ I_{ppf}^h \end{bmatrix}_{(m+n) \times 1} \quad (39)$$

Algorithm 1 was used to construct  $Z_{ppf}^h$  for the harmonic order  $h$ . The next step was to calculate the bus impedance matrix,  $M_S^h$ . After constructing  $Y_{bus}^h$  for the  $h$ -th harmonic order in OpenDSS,  $Y_{bus}^h$  was returned to MATLAB to obtain  $M_S^h$  by inverse matrix calculation.  $M_S^h$  is expressed as

$$(Y_{bus}^h)^{-1} = M_S^h = \begin{bmatrix} Z_{11}^h & \cdots & Z_{1i}^h \\ \vdots & \ddots & \vdots \\ Z_{i1}^h & \cdots & Z_{ii}^h \end{bmatrix}_{i \times i} \quad (40)$$

Therefore, (28) can be rewritten as (41):

$$V_{bus}^h = M_S^h \cdot I_{bus}^h \quad (41)$$

$\mathbf{V}_{ppf}^h$  is obtained from  $\mathbf{V}_{bus}^h$  using (42). Here,  $\mathbf{M}_F^h$  is the full coefficient matrix. It can be decomposed into the nonlinear load coefficient matrix  $\mathbf{M}_L^h$  and PPFs coefficient matrix  $\mathbf{M}_{ppf}^h$ .

$$\mathbf{V}_{ppf}^h = \mathbf{M}_F^h \cdot \mathbf{I}_S^h = \begin{bmatrix} \mathbf{M}_L^h & \mathbf{M}_{ppf}^h \end{bmatrix} \begin{bmatrix} \mathbf{I}_L^h \\ \mathbf{I}_{ppf}^h \end{bmatrix} \quad (42)$$

Unlike the FPF, the HPF considers the direction of the harmonic current flowing into the power system. Therefore,  $\mathbf{V}_{ppf}^h$  can be represented as follows:

$$\mathbf{V}_{ppf}^h = -\mathbf{Z}_{ppf}^h \cdot \mathbf{I}_{ppf}^h \quad (43)$$

Substituting (43) into (42) yields  $\mathbf{I}_{ppf}^h$  as

$$\mathbf{I}_{ppf}^h = -(\mathbf{Z}_{ppf}^h + \mathbf{M}_{ppf}^h)^{-1} \cdot \mathbf{M}_L^h \cdot \mathbf{I}_L^h \quad (44)$$

After constructing  $\mathbf{I}_{ppf}^h$  in MATLAB, it was returned to OpenDSS, and a current source was established at the corresponding bus. The injection current source vector  $\mathbf{I}_{inj}^h$  is given by (45):

$$\mathbf{I}_{inj}^h = \begin{bmatrix} I_{inj,1}^h \\ \vdots \\ I_{inj,i}^h \end{bmatrix}_{i \times 1} \quad (45)$$

Then, the injection current vector  $\mathbf{I}_{inj}^h$  obtained from MATLAB and bus current vector  $\mathbf{I}_{bus}^h$  obtained from OpenDSS were combined to form the total harmonic current vector  $\mathbf{I}_{bus}^h$ . It was used to solve the internal HPF in OpenDSS as illustrated in (46):

$$\mathbf{V}_{bus}^h = \mathbf{M}_S^h \cdot \begin{bmatrix} \mathbf{I}_{bus}^h + \mathbf{I}_{inj}^h \end{bmatrix} \quad (46)$$

A coefficient matrix can be constructed based on the voltage index (VID) and current index (CID). The construction rules for VID and CID are as follows:

VID is the node number vector where the PPF equivalent injection current source is installed on the corresponding bus. This is expressed in (47):

$$\mathbf{VID} = \begin{bmatrix} \text{node}_{Z_{ppf,1}^h} \\ \vdots \\ \text{node}_{Z_{ppf,n}^h} \end{bmatrix}_{n \times 1} \quad (47)$$

CID is the node number vector where the harmonic load is installed on the corresponding bus, as shown in (48):

$$\mathbf{CID} = \begin{bmatrix} \text{node}_{I_{L,1}^h} \\ \vdots \\ \text{node}_{I_{L,n}^h} \end{bmatrix}_{m \times 1} \quad (48)$$

VID was constructed using MATLAB based on the locations of the PPFs. The current source data were transmitted from OpenDSS to MATLAB via a COM interface to construct CID. After constructing the two index vectors,  $\mathbf{M}_L^h$  and  $\mathbf{M}_{ppf}^h$  were determined according to the VID and CID. The node numbers in the VID determine the row elements of  $\mathbf{M}_L^h$  and

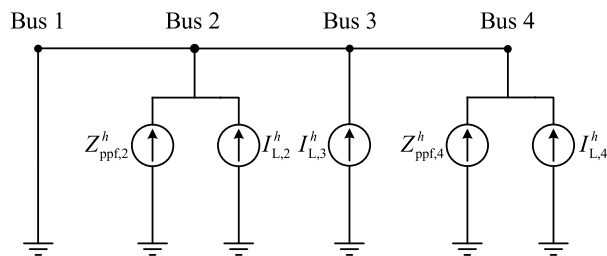


FIGURE 9. A radial system with two PPFs and three harmonic loads.

the row and column elements of  $\mathbf{M}_{ppf}^h$ . The number of nodes in the CID determines the column elements of  $\mathbf{M}_L^h$ .

According to the rules, the following is obtained after elements are selected from  $\mathbf{M}_S^h$ :

$$\mathbf{M}_L^h = \begin{bmatrix} Z_{\text{node}_{Z_{ppf,1}^h} \text{ node}_{I_{L,1}^h}} & \cdots & Z_{\text{node}_{Z_{ppf,1}^h} \text{ node}_{I_{L,m}^h}} \\ \vdots & \ddots & \vdots \\ Z_{\text{node}_{Z_{ppf,n}^h} \text{ node}_{I_{L,1}^h}} & \cdots & Z_{\text{node}_{Z_{ppf,n}^h} \text{ node}_{I_{L,m}^h}} \end{bmatrix}_{n \times m} \quad (49)$$

and

$$\mathbf{M}_{ppf}^h = \begin{bmatrix} Z_{\text{node}_{Z_{ppf,1}^h} \text{ node}_{Z_{ppf,1}^h}} & \cdots & Z_{\text{node}_{Z_{ppf,1}^h} \text{ node}_{Z_{ppf,n}^h}} \\ \vdots & \ddots & \vdots \\ Z_{\text{node}_{Z_{ppf,n}^h} \text{ node}_{Z_{ppf,1}^h}} & \cdots & Z_{\text{node}_{Z_{ppf,n}^h} \text{ node}_{Z_{ppf,n}^h}} \end{bmatrix}_{n \times n} \quad (50)$$

Figure 9 shows a simple radial power system with two PPFs and three harmonic loads used to demonstrate the construction of the coefficient matrix. Bus 1 is regarded as the swing bus. The swing bus is grounded during the HPF.

According to Figure 9, the corresponding VID and CID are

$$\mathbf{VID} = \begin{bmatrix} 2 \\ 4 \end{bmatrix} \quad (51)$$

and

$$\mathbf{CID} = \begin{bmatrix} 2 \\ 3 \\ 4 \end{bmatrix} \quad (52)$$

According to the rules,  $\mathbf{M}_L^h$  and  $\mathbf{M}_{ppf}^h$  are

$$\mathbf{M}_L^h = \begin{bmatrix} Z_{22}^h & Z_{23}^h & Z_{24}^h \\ Z_{42}^h & Z_{43}^h & Z_{44}^h \end{bmatrix} \quad (53)$$

and

$$\mathbf{M}_{ppf}^h = \begin{bmatrix} Z_{22}^h & Z_{24}^h \\ Z_{42}^h & Z_{44}^h \end{bmatrix} \quad (54)$$

After calculating  $\mathbf{V}_{bus}^h$ , the harmonic indices of the power system can be evaluated according to (5)–(7). A flowchart of the direct  $Z_{BUS}$  harmonic power flow is shown in Figure 10, and the pseudocode is shown in Figure 11.



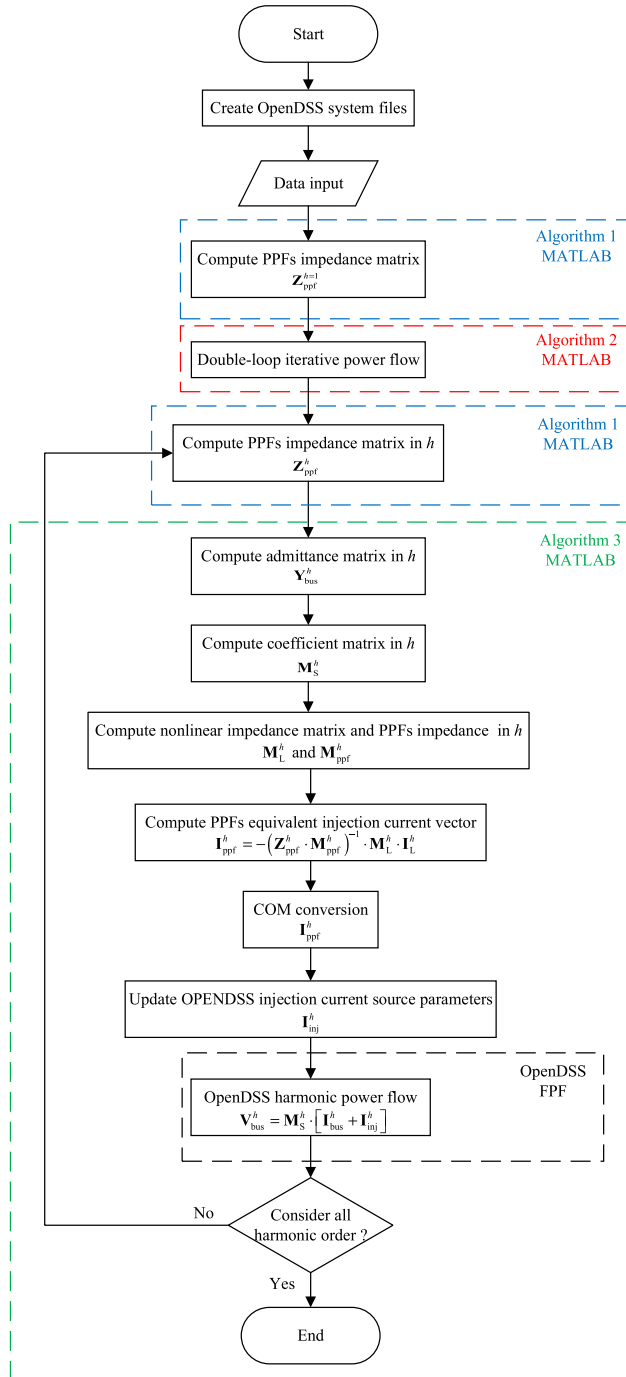


FIGURE 10. Flow chart of direct  $Z_{BUS}$  harmonic power flow.

### 3) $G_I^h$ SCANNING METHOD

In the conventional frequency scanning method [18], a scanning current source is installed at the observed bus to measure its impedance response of the observed bus with respect to frequency. Because the PPFs model proposed in this study is a current source rather than an impedance form, the conventional frequency scanning method cannot be applied to the proposed PPFs model. Therefore, the  $G_I^h$  scanning method has been proposed as an alternative to the traditional frequency-scanning methods.

### Algorithm 3 Direct $Z_{BUS}$ harmonic power flow

**Input:**  $Z_{ppf}^h$  and  $Y_{bus}^h$

**Output:**  $V_{bus}^h$

- 1: Read  $Z_{ppf}^h$  and  $Y_{bus}^h$
- 2:  $Y_{bus}^h$  return to MATLAB to calculate  $M_S^h \leftarrow$  Eqn. (40)
- 3: Build **VID** based on the locations of PPFs  $\leftarrow$  Eqn. (47)
- 4: Build **CID** based on harmonic loads  $\leftarrow$  Eqn. (48)
- 5: Build  $M_L^h$  based on **CID**  $\leftarrow$  Eqn. (49)
- 6: Build  $M_{ppf}^h$  based on **VID**  $\leftarrow$  Eqn. (50)
- 7: Calculate  $I_{ppf}^h \leftarrow$  Eqn. (44)
- 8:  $I_{ppf}^h$  return to OpenDSS  $\triangleright$  build  $I_{inj}^h \leftarrow$  Eqn. (45)
- 9:  $I_{bus}^h + I_{inj}^h$
- 10: Execute HPF of OpenDSS  $\triangleright$  calculate  $V_{bus}^h \leftarrow$  Eqn. (46)
- 11: Consider all harmonic order. If not  $\triangleright$  repeat Step 1
- 12: **Output:**  $V_{bus}^h$

FIGURE 11. Pseudo-code-for Algorithm 3.

The scenario setting of the  $G_I^h$  scanning method is similar to that of the conventional frequency-scanning method. All the loads are open circuit. A scanning current source,  $I_{scan}^h$  is installed at the observed bus. In this scenario, the only currents flowing at the observed bus are  $I_{scan}^h$  and  $I_{ppf}^h$ . Therefore, the observed bus  $G_I^h$  can be expressed as (55):

$$G_I^h = \frac{|I_S^h|}{|I_L^h|} = \frac{|I_{ppf}^h + I_{scan}^h|}{|I_{scan}^h|} \quad (55)$$

The subsequent steps are similar to those described in Algorithm 3. After obtaining the coefficient matrix,  $I_{ppf}^h$  was calculated.  $I_{ppf}^h$  returns to OpenDSS to perform HPF and calculate  $I_S^h$ . Hence, the  $G_I^h$  at the observed bus can be evaluated using (55). A flowchart of the  $G_I^h$  scanning method is shown in Figure 12 and the pseudocode is shown in Figure 13.

## V. RESULT AND DISCUSSION

This study demonstrated the accuracy and practicality of the proposed PPFs model and algorithm using two test systems. The first test system validated the effectiveness of the  $G_I^h$  scanning method. Meanwhile, the second test system verified the double-loop iterative power flow and the direct  $Z_{BUS}$  harmonic power flow.

### A. CASE STUDY1

The small test system proposed in [11] was used. A single-tuned PPF model in OpenDSS was installed on bus 3, as shown in Figure 14.

The parameters of the test system are listed in Table 1. All the impedance parameters were calculated using the fundamental frequency.

For a sample system with buses 1 and 3 as the observed buses, the driving-point impedance can be calculated directly. The expression for the driving-point impedance  $Z_{11}^h$  at the harmonic order  $h$  is

$$Z_{11}^h = Z_{sys}^h // \frac{1}{h \cdot B_1} // \left\{ Z_{L,1}^h + Z_{L,2}^h + \left( \frac{1}{h \cdot B_3} // Z_{ppf}^h \right) \right\} \quad (56)$$

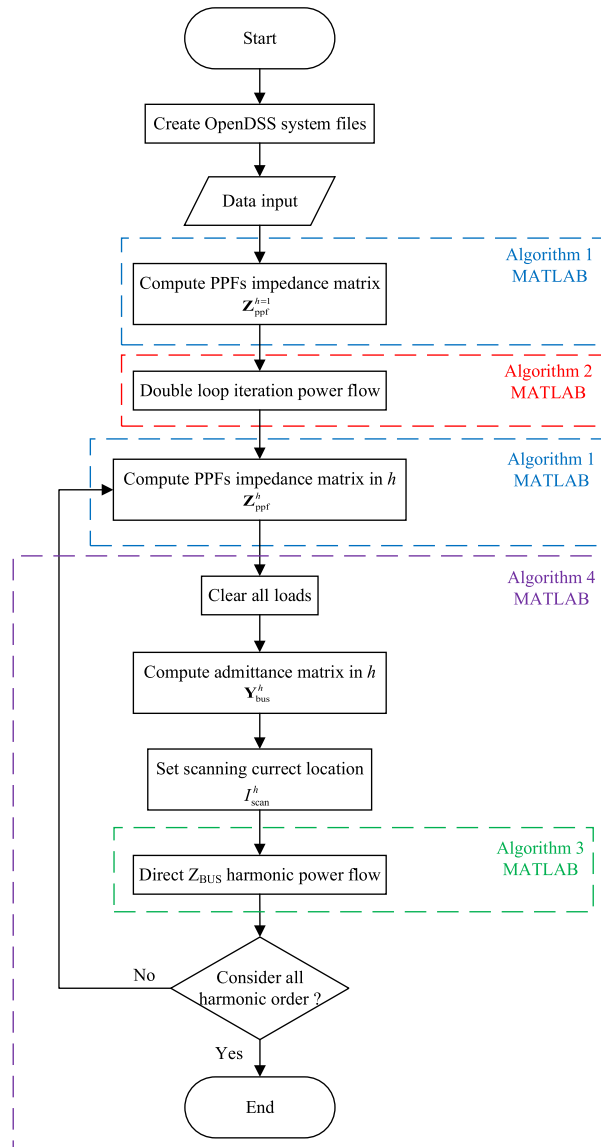


FIGURE 12. Flow chart of the  $G_1^h$  scanning method.

TABLE 1. Small test system parameters.

Item	Impedance (pu)
$Z_{sys}$	$0.04+j0.3$
$Z_{L,1}$	$0.835+j4$
$Z_{L,2}$	$0.835+j4$
$B_1$	$j0.0013$
$B_2$	$j0.0013$
$Z_{ppf}$	$j0.9504-j46.5726$

The  $Z_{33}^h$  at the harmonic order  $h$  is

$$Z_{33}^h = \left\{ \left( Z_{sys}^h // \frac{1}{h \cdot B_1} \right) + Z_{L,1}^h + Z_{L,2}^h \right\} // \frac{1}{h \cdot B_3} // Z_{ppf}^h \quad (57)$$

Using the conventional frequency scanning method, the frequency scan range was set to 1–60 pu with a precision

**Algorithm 4**  $G_1^h$  scanning method

- Input:**  $I_{scan}^h$  data,  $Z_{ppf}^h$  and  $Y_{bus}^h$   
**Output:**  $G_1^h$  scan image
- 1: Read  $I_{scan}^h$
  - 2: Read  $Z_{ppf}^h$  and  $Y_{bus}^h$
  - 3: Execute Algorithm 3 direct  $Z_{BUS}$  harmonic power flow
  - 4: Consider all harmonic order. If not  $\triangleright$  repeat Step 2
  - 5: Plot all  $G_1^h$  on the XY-axis //  $G_1^h$  scan image
  - 6: **Output:**  $G_1^h$  scan image

FIGURE 13. Pseudo-code for algorithm 4.

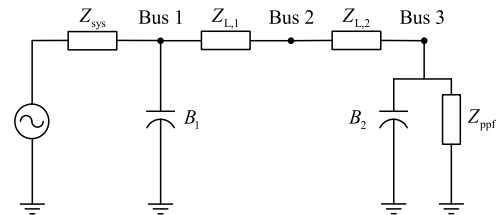


FIGURE 14. Small test system.

TABLE 2. Comparison for calculated and OpenDSS results.

Item	Calculated		OpenDSS	
Resonance frequency (pu)	30.73	51.62	30.73	51.62
$Z_{11}^h$ (pu)	121.86	5348.72	70.05	5202.01
$Z_{33}^h$ (pu)	38216.73	26.47	36495.52	31.85

of 0.01 Hz. The scan results showed that harmonic resonances occurred at buses 1 and 3 at frequencies of 30.73 pu and 51.62 pu, respectively. The harmonic resonance frequencies were substituted into (56) and (57) to calculate the driving-point impedances  $Z_{11}^h$  and  $Z_{33}^h$ . The comparison results between the frequency scan and direct calculation are listed in Table 3.

The comparison results in Table 2 reveal that when the power system experiences harmonic resonance, the results obtained using the conventional frequency-scanning method differ significantly from those obtained by the direct calculation. Because  $Y_{bus}$  becomes a singular matrix, OpenDSS cannot accurately solve the inverse matrix. This observation supports the concept that the voltage solutions obtained by the HPF in OpenDSS cause inaccuracies owing to impedance errors in power systems with harmonic resonances.

Therefore, the  $G_1^h$  scanning method proposed in this study was used for harmonic resonance analysis. The scan frequency range was 1–60 pu, with a precision of 0.01 Hz. The  $G_1^h$  scan results for OpenDSS with a single-tuned PPF model are shown in Figure 15.

The  $G_1^h$  scan results obtained after replacing the proposed PPFs model are shown in Figure 16.

Table 3 compares the proposed PPFs model and single-tuned PPF model in OpenDSS for  $G_1^h$  at the harmonic resonance frequencies.

Based on the  $G_1^h$  scan diagram, it can be verified that the extremum of  $G_1^h$  occurs at the harmonic resonance frequency of the power system. This corresponds to the results obtained

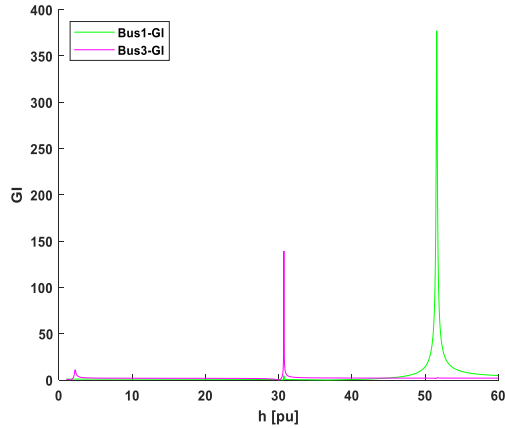


FIGURE 15.  $G_1^h$  scan result with OpenDSS PPF model.

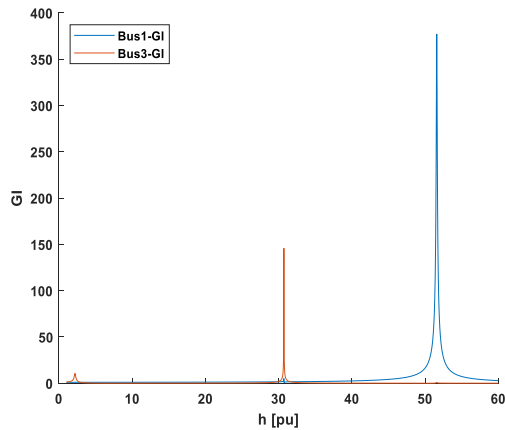


FIGURE 16.  $G_1^h$  scan result with proposed model.

using the OpenDSS model. The  $G_1^h$  values differed because of errors in the inverse matrix calculation performed by OpenDSS. These results demonstrate that the proposed  $G_1^h$  scanning method can accurately identify harmonic resonance frequencies in power systems. Moreover,  $G_1^h$  is a better indicator of the severity of harmonic resonance in a power system than the driving-point impedance.

**B. CASE STUDY2**

The second test system used in this study was the Taipower 38 bus test system obtained from a previous study [19] (see Figure 17). The harmonic spectrum of a typical non-linear load is shown in Table 4. The other relevant parameters were obtained from [19]. The SCs and PPFs were installed in the Taipower distribution system, and the point of common coupling (PCC) was located at bus 36. The accuracies of the double-loop iterative power flow and direct  $Z_{BUS}$  harmonic power flow methods proposed in this study were verified.

**1) SCENARIO 1**

No shunt components (SCs and PPFs) were present in the original system configuration. The harmonic load was distributed among various buses. The fundamental voltage at the buses is shown in Figure 18 (a) as a blue curve. It indicates

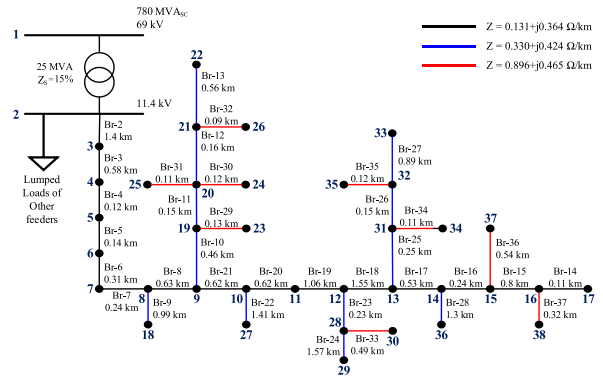


FIGURE 17. Taipower 38 bus distribution system.

TABLE 3. Comparison for proposed model and OpenDSS results.

Item	Proposed model		OpenDSS	
Resonance frequency (pu)	30.73	51.62	30.73	51.62
Bus 1- $G_1^h$	0.62	376.94	3.51	377.01
Bus 3- $G_1^h$	145.64	0.78	139.17	2.40

TABLE 4. Typical harmonic spectrum.

Harmonic order	Typical harmonic spectrum	
	$I_{\text{spectrum}}^h$ (%)	$\theta_{\text{spectrum}}^h$ (°)
1	100	0
5	18.24	-55.68
7	11.90	-84.11
11	5.73	-143.56
13	4.01	-175.58
17	1.93	111.39
19	1.39	68.30
23	0.94	-24.61
25	0.86	-67.64
29	0.71	-145.46
31	0.62	176.83
35	0.44	97.40
37	0.38	54.36

that the voltage decreases as the distance from the bus increases. Because there were no shunt components to prevent harmonic current in the power system, the TVHD at each bus is shown in Figure 18(b) as a blue curve. The TVHD at the PCC was recorded as 3.82%.

**2) SCENARIO 2**

In Scenario 2, SCs were installed at buses 14, 16, 36, 37, and 38. The fundamental voltages at the buses are shown in Figure 18 (a) as red curves. The fundamental voltage was not significantly different from that in Scenario 1. However, owing to the harmonic resonance of the SCs, the TVHD at each bus is shown in Figure 18 (b) as a red curve, indicating the amplification of the TVHD at each bus. The TVHD at the PCC is 6.41%.

**3) SCENARIO 3**

PPFs were installed on the buses to improve the harmonic pollution, with a second-order PPF at Bus 16, third-order PPF at Bus 36, and C-type PPF at Bus 27. The fundamental

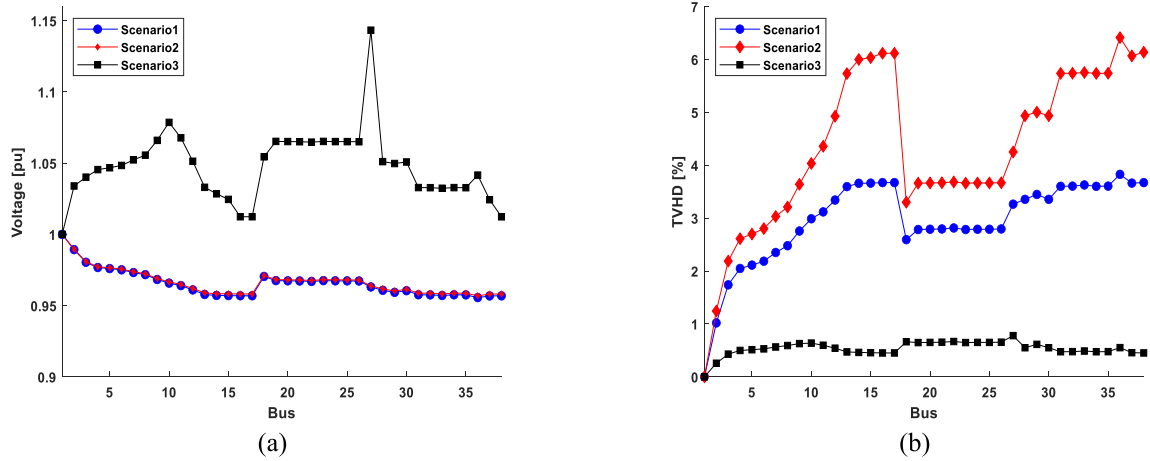


FIGURE 18. (a) Fundamental bus voltage (b) TVHD of bus.

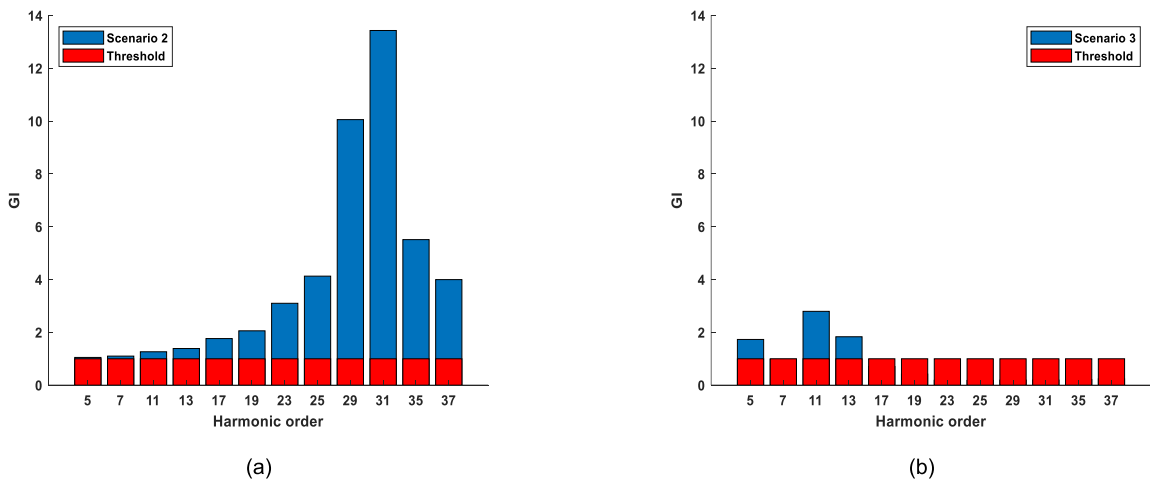


FIGURE 19. Box charts of (a)  $G_1^h$  at PCC in scenario 2 (b)  $G_1^h$  at PCC in scenario 3.

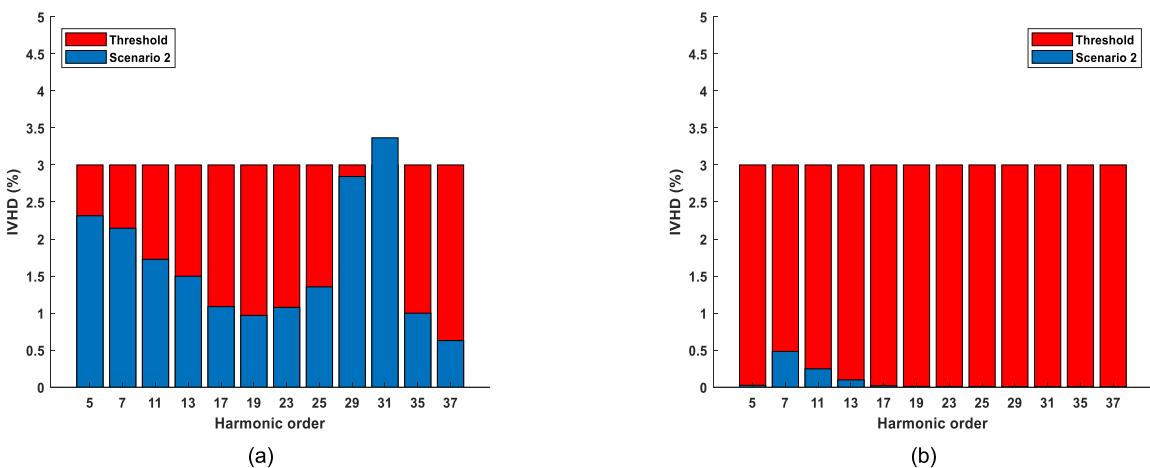


FIGURE 20. Box charts of (a)  $IVHD^h$  at PCC in scenario 2 (b)  $IVHD^h$  at PCC in scenario 3.

voltage was calculated using the double-loop iterative power flow proposed in this study and was compared with the results

in [19] (see Table 5). The fundamental voltage curve is shown in Figure 18 (a) as a black curve. It can be observed that

TABLE 5. Accuracy comparison for PPF in scenario3.

Bus	Voltage [pu]∠rad		Bus	Voltage [pu]∠rad		Bus	Voltage [pu]∠rad	
	Proposed method	[19]		Proposed method	[19]		Proposed method	[19]
1	1∠0	1∠0	14	1.028∠-0.63	1.028∠-0.63	27	1.140∠-0.49	1.140∠-0.49
2	1.034∠-0.18	1.034∠-0.18	15	1.024∠-0.63	1.025∠-0.63	28	1.051∠-0.52	1.051∠-0.52
3	1.040∠-0.27	1.040∠-0.27	16	1.012∠-0.67	1.012∠-0.67	29	1.049∠-0.53	1.049∠-0.53
4	1.045∠-0.31	1.045∠-0.31	17	1.012∠-0.67	1.012∠-0.67	30	1.050∠-0.53	1.050∠-0.53
5	1.046∠-0.32	1.047∠-0.32	18	1.054∠-0.37	1.054∠-0.37	31	1.033∠-0.60	1.033∠-0.60
6	1.048∠-0.33	1.048∠-0.33	19	1.065∠-0.4	1.065∠-0.40	32	1.033∠-0.60	1.033∠-0.60
7	1.052∠-0.35	1.052∠-0.35	20	1.065∠-0.4	1.065∠-0.40	33	1.032∠-0.60	1.032∠-0.60
8	1.055∠-0.36	1.056∠-0.36	21	1.065∠-0.4	1.065∠-0.40	34	1.033∠-0.60	1.033∠-0.60
9	1.066∠-0.41	1.066∠-0.41	22	1.064∠-0.41	1.065∠-0.41	35	1.033∠-0.60	1.033∠-0.60
10	1.078∠-0.44	1.078∠-0.44	23	1.065∠-0.41	1.065∠-0.41	36	1.042∠-0.63	1.042∠-0.63
11	1.067∠-0.47	1.067∠-0.47	24	1.065∠-0.41	1.065∠-0.41	37	1.024∠-0.63	1.024∠-0.63
12	1.051∠-0.52	1.051∠-0.52	25	1.065∠-0.41	1.065∠-0.41	38	1.012∠-0.67	1.012∠-0.67
13	1.033∠-0.6	1.033∠-0.6	26	1.065∠-0.41	1.065∠-0.41			

TABLE 6. Accuracy comparison for HPF in scenario3.

Bus	TVHD [%]		Bus	TVHD [%]		Bus	TVHD [%]	
	Proposed method	[19]		Proposed method	[19]		Proposed method	[19]
1	0	0	14	0.461	0.461	27	0.778	0.778
2	0.257	0.257	15	0.456	0.456	28	0.550	0.550
3	0.428	0.428	16	0.451	0.451	29	0.613	0.613
4	0.498	0.498	17	0.451	0.451	30	0.550	0.550
5	0.512	0.512	18	0.663	0.663	31	0.474	0.474
6	0.528	0.528	19	0.647	0.647	32	0.476	0.476
7	0.564	0.564	20	0.651	0.651	33	0.487	0.487
8	0.591	0.591	21	0.654	0.654	34	0.474	0.474
9	0.628	0.628	22	0.667	0.667	35	0.476	0.476
10	0.637	0.637	23	0.647	0.647	36	0.551	0.551
11	0.596	0.596	24	0.651	0.651	37	0.456	0.456
12	0.541	0.541	25	0.651	0.651	38	0.451	0.451
13	0.471	0.470	26	0.654	0.654			

the voltage increased significantly when SCs and PPFs were installed in the power system.

The TVHD at each bus was calculated using the direct  $Z_{BUS}$  harmonic power flow proposed in this study and compared with the results in [19] (see Table 6). The TVHD curve is shown in Figure 18 (b) as the black curve. It can be observed that the installation of PPFs could mitigate harmonic pollution and thereby, cause a significant decrease in the TVHD at each bus.

The results of the double-loop iterative power flow and direct  $Z_{BUS}$  harmonic power flow proposed in this study were observed to be consistent with those in [19]. This verified the high accuracy of the proposed methods. Thus, the proposed PPFs model can be applied to practical distribution systems.

In addition, the  $G_1^h$  at the PCC could be observed, as shown in Figure 19 (a). The red line represents a  $G_1^h$  value of one.  $G_1^h$  indicates harmonic current amplification if it is exceeded. The box chart shows that harmonic amplification occurs after the 17th harmonic order when only SCs are installed in the power system. The IVHD at the PCC is shown in Figure 20 (a).

It can be verified that the IVHD of the 29th and 31st harmonic orders are significantly higher than those of the other orders owing to harmonic amplification. Moreover, the IVHD of the 31st harmonic order exceeds the 3% limit specified by IEEE Standard 519-2014 [20] (red line).

As shown in Figure 19 (b), installing PPFs significantly reduced the harmonic amplification in the power system. Furthermore, as shown in Figure 20 (b), the IVHD of each harmonic order at the PCC decreased and satisfied the limit of IEEE Standard 519-2014.  $G_1^h$  provides a more accurate assessment of the harmonic resonance of a system.

VI. CONCLUSION

The method proposed in this study combines the equivalent injection current-based PPFs model with the dual-loop iterative power flow and direct  $Z_{BUS}$  harmonic power flow. It performs harmonic analysis and PPF design in OpenDSS. The method overcomes the limitations of OpenDSS in high-order filter models and the HPF calculation errors owing to harmonic resonance. Two test systems were used to demon-



strate the accuracy of the proposed PPFs model and method. The  $G_1^h$  harmonic current gain indicator was introduced as a tool to evaluate the resonance between the shunt components and power system. Overall, this study provided a comprehensive and accurate method for harmonic analysis and PPF design in practical distribution systems.

## REFERENCES

- [1] R. C. Dugan, *Electrical Power Systems Quality*, 2nd ed. New York, NY, USA: McGraw-Hill, 2003.
- [2] J. Grainger and S. Lee, "Optimum size and location of shunt capacitors for reduction of losses on distribution feeders," *IEEE Trans. Power App. Syst.*, vols. PAS-100, no. 3, pp. 1105–1118, Mar. 1981.
- [3] Y. Baghzouz, "Effects of nonlinear loads on optimal capacitor placement in radial feeders," *IEEE Trans. Power Del.*, vol. 6, no. 1, pp. 245–251, Jan. 1991.
- [4] N. Chang, "Locating shunt capacitors on primary feeder for voltage control and loss reduction," *IEEE Trans. Power App. Syst.*, vols. PAS-88, no. 10, pp. 1574–1577, Oct. 1969.
- [5] D. Çelik, "Lyapunov based harmonic compensation and charging with three phase shunt active power filter in electrical vehicle applications," *Int. J. Electr. Power Energy Syst.*, vol. 136, Mar. 2022, Art. no. 107564.
- [6] S. H. Hamouda, S. H. E. A. Aleem, and A. M. Ibrahim, "Harmonic resonance index and resonance severity estimation for shunt capacitor applications in industrial power systems," in *Proc. 19th Int. Middle East Power Syst. Conf. (MEPCON)*, 2017, pp. 527–532.
- [7] W. Xu, J. R. Marti, and H. W. Dommel, "A multiphase harmonic load flow solution technique," *IEEE Power Eng. Rev.*, vol. 11, no. 2, p. 54, Feb. 1991.
- [8] Y. H. Yan, C. S. Chen, C. S. Moo, and C. T. Hsu, "Harmonic analysis for industrial customers," *IEEE Trans. Ind. Appl.*, vol. 30, no. 2, pp. 462–468, Apr. 1994.
- [9] J.-H. Teng and C.-Y. Chang, "Backward/forward sweep-based harmonic analysis method for distribution systems," *IEEE Trans. Power Del.*, vol. 22, no. 3, pp. 1665–1672, Jul. 2007.
- [10] N. Yang and M. Le, "Three-phase harmonic power flow by direct  $Z_{BUS}$  method for unbalanced radial distribution systems with passive power filters," *IET Gener., Transmiss. Distribution*, vol. 10, no. 13, pp. 3211–3219, Oct. 2016.
- [11] W. Xu, Z. Huang, Y. Cui, and H. Wang, "Harmonic resonance mode analysis," *IEEE Trans. Power Del.*, vol. 20, no. 2, pp. 1182–1190, Apr. 2005.
- [12] R. C. Dugan and T. McDermott, "Reference guide, the open distribution system simulator (OpenDSS)," EPRI, Washington, DC, USA, 2016.
- [13] W. H. Kersting and R. K. Green, "The application of Carson's equation to the steady-state analysis of distribution feeders," in *Proc. IEEE/PES Power Syst. Conf. Expo.*, Mar. 2011, pp. 1–6.
- [14] D. Montenegro and R. Dugan, "How to speed up your co-simulation using OpenDSS COM interface," Washington, DC, USA, 2015.
- [15] T. Zhao, H. Chiang, and K. Koyanagi, "Convergence analysis of implicit Z-bus power flow method for general distribution networks with distributed generators," *IET Gener., Transmiss. Distribution*, vol. 10, no. 2, pp. 412–420, Feb. 2016.
- [16] T. A. Davis and E. Palamadai Natarajan, "Algorithm 907," *ACM Trans. Math. Softw.*, vol. 37, no. 3, pp. 1–17, 2010.
- [17] N. Yang, "Three-phase power flow calculations using direct  $Z_{BUS}$  method for large-scale unbalanced distribution networks," *IET Gener., Transmiss. Distribution*, vol. 10, no. 4, pp. 1048–1055, Mar. 2016.
- [18] X. Jiang and A. M. Gole, "A frequency scanning method for the identification of harmonic instabilities in HVDC systems," *IEEE Trans. Power Del.*, vol. 10, no. 4, pp. 1875–1881, Oct. 1995.
- [19] N. Yang and E. W. Adinda, "Matpower-based harmonic power flow analysis for power systems with passive power filters," *IEEE Access*, vol. 9, pp. 167322–167331, 2021.
- [20] *IEEE Recommended Practice and Requirements for Harmonic Control in Electric Power Systems*, New York, NY, USA, 1993.



**NIEN-CHE YANG** (Member, IEEE) was born in Keelung, Taiwan, in 1977. He received the B.S., M.S., and Ph.D. degrees in electrical engineering from the National Taiwan University of Science and Technology, Taipei, Taiwan, in 2002, 2004, and 2010, respectively. Since 2018, he has been a Faculty Member with the National Taiwan University of Science and Technology, where he is currently an Associate Professor of electrical engineering. His research interests include micro-grid state estimation, harmonic three-phase power flow analysis, probabilistic three-phase power flow analysis, energy loss computation in low voltage networks, microgrids, smart grids, and electric vehicles. He is a member of the Phi Tau Phi Scholastic Honor Society.



**YU-WEI HSU** was born in Taipei, Taiwan, in 2000. He received the B.S. degree from the National Taiwan University of Science and Technology (NTUST), Taipei, in 2022, where he is currently pursuing the M.S. degree with the Electrical Engineering Department. His research interests include power system analysis and harmonic analysis.